This is an preprint of an article published in Chemical Engineering Science 64 (23) 4835-4845 (2009).
DOI: http://dx.doi.org/10.1016/j.ces.2009.07.023. © copyright 2009 Elsevier Ltd.

Transient Rise Velocity and Mass Transfer of a Single Drop with Interfacial Instabilities - Numerical Investigations

M. Wegener[*,a], T. Eppinger[a], K. Bäumler[b], M. Kraume[a], A.R. Paschedag[c], E. Bänsch[a]

[a] *Chair of Chemical Engineering, Technische Universität Berlin, Ackerstraße 71-76, D-13355 Berlin, Germany*
[b] *Chair of Applied Mathematics III, Friedrich-Alexander-Universität, Erlangen-Nürnberg, Germany*
[c] *University of Applied Science Berlin, Luxemburger Str. 10, D-13353 Berlin, Germany*

Abstract

Full 3D-simulations of transient interfacial mass transfer accompanied by Marangoni convection at a single spherical droplet in a quiescent liquid were performed in a moving reference coordinate system. The flow and concentration field are solved simultaneously, coupled via the additional Marangoni stress generated by concentration gradients at the interface. Fluid dynamics and mass transfer are investigated in the Marangoni convection dominated toluene/acetone/water system. The numerical results are qualitatively and quantitatively compared with own experimental results. The simulation results reveal that mass transfer is always enhanced - compared to calculations where no Marangoni convection appears - independently from the initial solute concentration. The enhancement factor of mass transfer ranges between 2 and 3.

Key words: Marangoni convection, Mass transfer, Simulation, Drop, Extraction

1. Introduction

In the present numerical study, the influence of Marangoni convection on the transient mass transfer across the interface of liquid drops is investigated. Dispersed liquid-liquid systems play a major role in many engineering applications. For such dispersed systems with large interfacial contact area, a reliable prediction of mass transfer rates and relative velocities is required especially for the design of contactors. Many efforts have been made in order to describe the mass transfer to and from liquid drops both analytically (e.g. [1], [2], [3], [4], [5]) and numerically (e.g. [6], [7]).

Piarah et al. [8] and Paschedag et al. [9] presented sensitivity studies for systems with constant interfacial tension including the conjugated problem, i.e. mass transfer resistance in both phases, which applies particularly to liquid/liquid systems, and the two limiting cases where the mass transfer in one of the phases is infinitely fast (internal and external problem) without consideration of Marangoni convection. Results reveal the strong influence of the Peclet number on the mass transfer coefficient. Waheed et al. [10] investigated in their numerical simulations

[*] Corresponding Author
Email addresses: mirco.wegener@tu-berlin.de (M. Wegener), thomas.eppinger@tu-berlin.de (T. Eppinger), baeumler@am.uni-erlangen.de (K. Bäumler), matthias.kraume@tu-berlin.de (M. Kraume), anja.paschedag@tfh-berlin.de (A.R. Paschedag), baensch@mi.uni-erlangen.de (E. Bänsch)

the contributions of free and forced convection and the combination of both to the conjugated mass transfer problem using the finite element method (FEM).

In recent years, the mass transfer between deformable drops and a continuous phase with constant interfacial tension has been investigated intensely (e.g. [11], [12]). Other research groups investigated systems with high density ratio, i.e. hydrodynamics and/or mass transfer across the interface of bubbles in liquids using the volume of fluid technique (e.g. [13], [14], [15]) or the front tracking method ([16], [17], [18]). Koynov et al. [19] investigated hydrodynamic behaviour, mass transfer rates and chemical reactions in bubble swarms performing 2D-DNS simulations and compared different swarm configurations to a single bubble.

The numerical investigations of Mao et al. [20] focused on the external problem for deformable drops. Results show that mass transfer depends mainly on the Peclet number, followed by Reynolds number and Weber number. Yang and Mao [21] investigated the conjugated mass transfer using the level set approach with a decoupling algorithm. Results were compared with experiments and show reasonable agreement. A more accurate prediction with less deviance to experimental values was achieved in a recent work by Wang et al. [22]. In this work, flow and concentration field are coupled and the droplet acceleration after drop formation is considered. Mass transfer during the drop formation process is not included.

Many research groups dedicated their numerical work to the influence of insoluble surfactants on the flow around and on the mass transfer into single drops [23] or bubbles [24]. Li et al. [25] reported significant influence of surfactants on the drag coefficient and on the overall mass transfer coefficient. The surfactants lead to lower interfacial velocities which then decrease the local Sherwood numbers, especially in front of the sphere. In addition, surfactants seem to increase the interfacial mass transfer resistance. Compared to the pure system, this leads to a significantly reduced mass transfer coefficient.

In summary it can be ascertained that non-deformable drops without Marangoni convection can be described reliably. For deformable drops there are a couple of promising numerical techniques available.

When Marangoni convection appears, the physical behaviour of a system changes dramatically. Marangoni instabilities occur if the interfacial tension is a function of the local solute concentration at the interface. Additional flow patterns are generated and thus complex interactions between flow and concentration field. Both the internal circulation and the flow structure around the drop are affected and with this the overall mass transfer coefficient and the drag coefficient (e.g. [26]). To date, the phenomenon with all its interactions is not accessible to any analytical description. Hence, numerical methods have to be applied in order to investigate the effect of Marangoni instabilities on momentum and mass transfer. In a VOF-method presented by James and Lowengrub [27], the influence of Marangoni forces and the associated interfacial flows due to concentration gradients of an insoluble surfactant on a droplet in extensional flow is investigated. Wang et al. [28] computed the influence of surfactant transport on the velocity of a single bubble in axis-symmetric creeping flow using the Finite Difference Method. They found that the bubble velocity is significantly reduced when Marangoni effects become strong due to surface concentration gradients. Mao and Chen [29] studied numerically in 2D-simulations the influence of the Marangoni effect on mass transfer in a liquid-liquid system. They assumed an axis-symmetric laminar flow and spherical particle shape. Both mass transfer directions were investigated and compared with the linear stability analysis by Sternling and Scriven [30] with both agreement and disagreement which is obviously due to differing assumptions in both works. Plots of the Sherwood number as a function of time reveal that Marangoni convection appears in the middle stage of the mass transfer process. It needs some time to develop and disappears at the

end when the Sherwood number becomes constant. They showed that mass transfer is often but not always enhanced by Marangoni convection. The Marangoni flow patterns can be significant but unable to promote the mass transfer. They conclude that this behaviour mainly depends on the scale of the appearing roll cells, assuming that cells slightly smaller than the drop (so-called drop scale) are less effective than those significantly smaller than the drop (so-called sub-drop scale).

To our knowledge, no full 3D-simulations of mass transfer across the interface of moving drops with simultaneous Marangoni convection have been reported so far. Tryggvason et al. [16] investigated thermocapillary migration of three-dimensional bubbles assuming that the interfacial tension is a linear function of the temperature. Huo and Li [31] presented 3D-simulations of thermally induced Marangoni convection in electrostatically levitated drops using a finite element method. Results show complex 3D flow structures if the temperature gradient is not placed symmetrically at the poles.

The Marangoni effect is inherently three dimensional and unsteady. Own preliminary numerical investigations revealed that 2D-simulations were not capable of describing the effect of solutal Marangoni convection on mass transfer correctly [32]. In the present numerical study, 3D-simulations for a single moving spherical drop in a quiescent liquid are presented for cases where concentration gradients cause Marangoni convection. Flow and concentration fields are mutually coupled and solved simultaneously. Thus, drop rise velocity will depend on the strength of Marangoni convection. Initially, the drop is at rest, the changes in drop rise velocity are considered as a function of time. Mass transfer at the drop formation stage, however, is not included. The numerical results are compared with experimental investigations presented by Wegener et al. [33], namely with the transient drop rise velocity and the evolution of the mean solute concentration in the drop which were measured in the toluene/acetone/water system with variations in the initial solute concentration.

2. Numerical setup

For the simulations, the commercial CFD-code STAR-CD® (v3.24) by CD-adapco was used. The model domain is built close to the experimental conditions [33] and represents a section of the real apparatus, see Fig. 1. In the experiments, the dispersed phase (1) is pumped to a glass capillary (2) where the drop with a specified diameter (3) is formed. The drop rises in the column (4) with an inner diameter of 75 mm and is collected in a funnel device (5) for concentration measurements. In the simulations, the drop ($d_P = R/2 = 2\,mm$) is fixed in the middle of a cylindrical environment, which contains the surrounding fluid, with $d_{cyl}/R = 8$ and $h/d_{cyl} = 1$, see Fig. 2 (left). The continuous phase is regarded as an infinitely extended fluid, and the relative velocity between both phases is imposed by the inlet velocity (see 2.4 Boundary Conditions).

The computational domain dimensions were chosen as compact as possible and as large as necessary in order to find a good compromise between number of cells and model domain resolution. Fig. 2 (right) shows the local spherical coordinate system within the Cartesian reference coordinate system. The origin of the spherical coordinate system is situated in the centre of the droplet. The boundary conditions at the interface are advantageously formulated in the spherical coordinate system. The inlet velocity corresponds to the relative velocity between drop and surrounding fluid. Thus, for an external observer, the drop is at rest whereas the reference coordinate system is accelerated opposite to the inlet flow. In this way, the full movement of the drop through the experimental domain can be described except for the drop formation at the capillary and the drop collection in the funnel.

This is an preprint of an article published in Chemical Engineering Science 64 (23) 4835-4845 (2009).
DOI: http://dx.doi.org/10.1016/j.ces.2009.07.023. © copyright 2009 Elsevier Ltd.

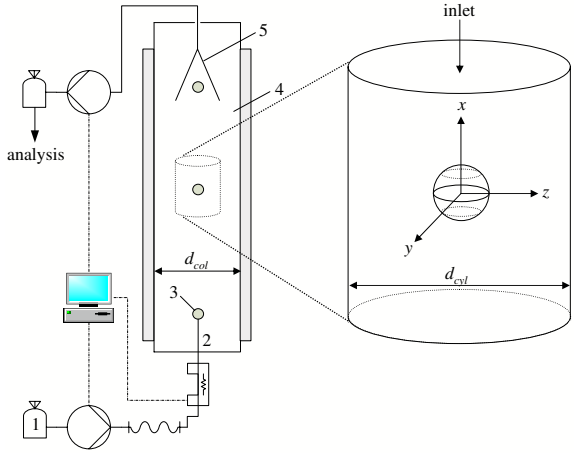

Fig. 1: Relation between experiments and computational domain. Simplified experimental setup: (1) dispersed phase, (2) capillary, (3) drop ($d_P = 2\,mm$ in this work), (4) column (with $d_P/d_{col} = 2/75 = 0.0266$), (5) funnel device. In the simulations, the drop is fixed in the middle of a cylindrical environment.

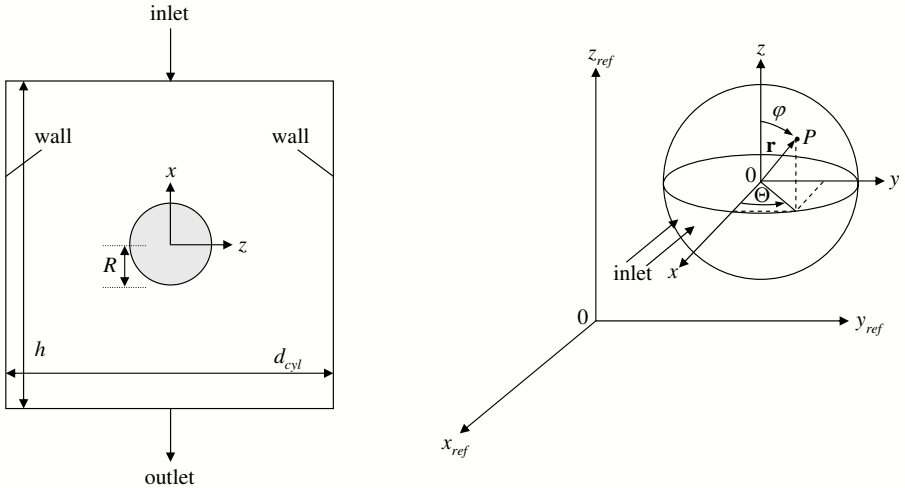

Fig. 2: Left: Length ratios of the model. x,z-plane in global Cartesian coordinates, $h/d_{cyl} = 1$. $d_{cyl}/R = 8$. Right: Relationship between reference coordinate system and local spherical coordinate system with $0 \leq \Theta \leq 2\pi$, $0 \leq \varphi \leq \pi$.

This is an preprint of an article published in Chemical Engineering Science 64 (23) 4835-4845 (2009).
DOI: http://dx.doi.org/10.1016/j.ces.2009.07.023. © copyright 2009 Elsevier Ltd.

In Table 1, the physical parameters of the system published by Misek et al. [34] are summarized. Toluene is the dispersed phase, water the continuous phase, acetone is the solute. The initial concentration of the solute in the droplet, $c_{A,0}$, varies between 0.01 and 30 g/L in the numerical studies whereas in the experiments the lower limit is 0.9 g/L. The mass transfer direction is from the dispersed to the continous phase ($d \rightarrow c$), the drop diameter is fixed to $d_P = 2\,mm$.

Table 1: Physical parameters for $\vartheta = 25^{\circ}$C.

	ρ [kg/m^3]	μ [$10^{-4}\cdot$ Pas]	D_A [$10^{-9}\cdot$ m^2/s]
Toluene$_{(d)}$	862.3	5.52	2.9
Water$_{(c)}$	997.02	8.903	1.25
Acetone$_{(A)}$	784.4	3.04	−−

2.1. Model simplification

In order to simplify the numerical analysis, some assumptions were made:

1. The drop is spherical, deformations are not considered.
2. The fluids are mutually immiscible.
3. The fluids are Newtonian and incompressible.
4. The transferred component is soluble in both phases and do not accumulate at the interface
5. Apart from the interfacial tension the physical properties are constant.
6. The drop moves vertically only.

The impact of the assumptions on the results are discussed at the end of the Results and discussion section.

2.2. Numerical grid and algorithm

The CFD-code is based on the finite volume method (FVM). The mesh consists entirely of hexahedral cells. Fig. 3 shows a section of the grid with zoom in the interfacial region. The grid specifications are listed in Table 2. The interface is resolved with 60 cells in Θ-direction and 32 cells in φ-direction. The thickness of the two cell layers adjacent to the interface is 1% of the drop radius. They play a major role for the discretization of the Eqs. (14), (17) and (18). Additionally, we perform test cases with a higher resolution of the interface (80x40 and 90x90 cells) and a higher corresponding total cell number (about 230000 cells and 600000 cells respectively) in order to justify the sensitivity of the simulations to grid refinements. Results show no significant improvement of the results, and thus, since the time to solution is increased likewise, the simulations with the grid specifications in Table 2 are favoured. Concerning the numerical algorithm, 2nd order discretisation in space and time has been used. The time derivatives are discretized with the Crank-Nicholson scheme whereas the convective terms have been discretized using the MARS scheme. MARS is a TVD limited 2nd order scheme developed by CD-adapco. The only specifications provided by the developer can be found in [35].

This is an preprint of an article published in Chemical Engineering Science 64 (23) 4835-4845 (2009).
DOI: http://dx.doi.org/10.1016/j.ces.2009.07.023. © copyright 2009 Elsevier Ltd.

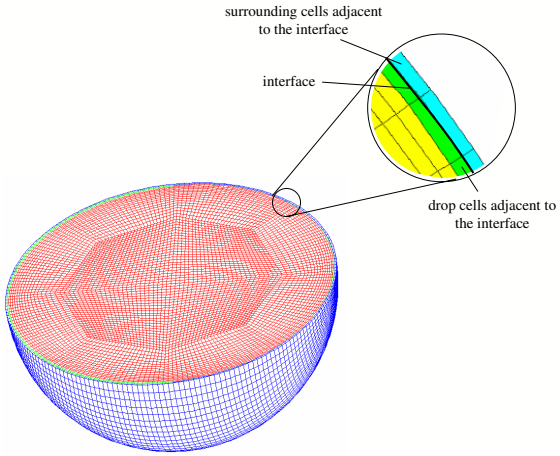

Fig. 3: Computational mesh of the drop (sectional view) and zoom in the interfacial region.

Table 2: Grid configuration.

number of interface cells in Θ-direction	60
number of interface cells in φ-direction	32
drop cells	47040
total number of cells	135360

2.3. Governing equations

In our FVM model, the Navier-Stokes equations, Eq. (1), are solved in each phase separately together with the continuity equation, Eq. (2). Note that the gravity force has been omitted in Eq. (1). It is included explicitely in the calculation for the inlet velocity, see next paragraph.

$$\rho\frac{\partial \mathbf{u}}{\partial t} + \rho\mathbf{u}\cdot\nabla\mathbf{u} + \nabla p - \mu\nabla^2\mathbf{u} = 0 \tag{1}$$

$$\nabla\cdot\mathbf{u} = 0 \tag{2}$$

The concentration of the transfer component is calculated via the mass balance equation, Eq. (3), which is coupled with the momentum balance and has to be solved for each phase as well:

$$\frac{\partial c_A}{\partial t} + \mathbf{u}\cdot\nabla c_A - D_A\nabla^2 c_A = 0 \tag{3}$$

This is an preprint of an article published in Chemical Engineering Science 64 (23) 4835-4845 (2009).
DOI: http://dx.doi.org/10.1016/j.ces.2009.07.023. © copyright 2009 Elsevier Ltd.

2.4. Boundary conditions

Wall

As shown in Fig. 1, the outer wall of the computational domain lies within the continuous phase in the experiments and hence is not equal with the real column wall. Therefore, the slip condition has been applied for the "wall" boundary which is been considered the best approximation to describe a cut through an extended fluid.

Inlet velocity

From the perspective of the moving computational domain, the continuous phase flows through the domain. Therefore, the inlet velocity needs to be determined from the velocity of the domain which is equal to the drop velocity. The transformation of Eqs. (1) and (2) to the moving reference frame leads to the appearance of an additional term which becomes zero when the drop reaches its steady rise velocity. Since there is no direct access to the momentum equation in STAR-CD, an explicit treatment based on the force balance at the drop surface is necessary. Therefore, a modified pressure is derived from the transformation of the "reference coordinate system" to the "drop coordinate system". "Reference coordinate system" in this case is a coordinate system relative to a fixed observer. The modified pressure is then incorporated into Newton's 2nd law to calculate the relative velocity between drop and surrounding fluid.

Denote the "drop coordinate system" by $\vec{\mathbf{x}} = x, y, z$, and the "reference coordinate system" by $\vec{\mathbf{x}}_{ref} = x_{ref}, y_{ref}, z_{ref}$, see Fig. 2 (right). Since only the movement in x-direction is considered, we have $y = y_{ref}$ and $z = z_{ref}$. The transformation is such that the centre of the droplet in the drop coordinate system is fixed to the origin for all times. The drop coordinate system is defined via a time dependent transformation Φ of the reference coordinate system:

$$\vec{\mathbf{x}} := \Phi(\vec{\mathbf{x}}_{ref}, t) = (x_{ref}, y_{ref}, z_{ref}) - x_{sp}(t)\vec{e}_x \tag{4}$$

where $x_{sp}(t)$ is the time dependent x-coordinate of the centre of the droplet in the reference coordinate system. We define the corresponding velocity $\mathbf{u}(\vec{\mathbf{x}}, t)$ and pressure $p(\vec{\mathbf{x}}, t)$ for the respective phase:

$$\mathbf{u}(\vec{\mathbf{x}}, t) := \mathbf{u}_{ref}(\vec{\mathbf{x}}_{ref}, t) - \dot{x}_{sp}\vec{e}_x \tag{5a}$$
$$p(\vec{\mathbf{x}}, t) := p_{ref}(\vec{\mathbf{x}}_{ref}, t) + \rho\ddot{x}_{sp}\vec{e}_x \cdot \vec{\mathbf{x}}_{ref} \tag{5b}$$

By Eq. (5), the partial derivatives with respect to time become

$$\frac{\partial \mathbf{u}(\vec{\mathbf{x}}, t)}{\partial t} = \frac{\partial \mathbf{u}_{ref}(\vec{\mathbf{x}}_{ref}, t)}{\partial t} + \frac{\partial \mathbf{u}_{ref}(\vec{\mathbf{x}}_{ref}, t)}{\partial x}\dot{x}_{sp}\vec{e}_x - \ddot{x}_{sp}\vec{e}_x. \tag{6}$$

The momentum equation for the reference coordinate system writes, omitting the gravitational force on the right hand side:

$$\rho\left(\frac{\partial \mathbf{u}_{ref}}{\partial t} + \mathbf{u}_{ref} \cdot \nabla_{ref}\mathbf{u}_{ref}\right) - \mu\nabla^2_{ref}\mathbf{u}_{ref} + \nabla_{ref}p_{ref} = 0 \tag{7}$$

This is an preprint of an article published in Chemical Engineering Science 64 (23) 4835-4845 (2009).
DOI: http://dx.doi.org/10.1016/j.ces.2009.07.023. © copyright 2009 Elsevier Ltd.

By Eqs. (5) and (6), Eq. (7) is transformed to the drop coordinate system:

$$\rho\left(\frac{\partial \mathbf{u}}{\partial t} + \mathbf{u}\cdot\nabla\mathbf{u}\right) - \mu\nabla^2\mathbf{u} + \nabla p = 0 \tag{8}$$

with the additional source term $\rho\ddot{x}_{sp}\vec{e}_x\cdot\vec{\mathbf{x}}_{ref}$ "hidden" in the pressure p. The modified pressure is then used in the force balance which in turn is used for the calculation of the inlet velocity. Buoyancy and gravitational force are independent from the flow and pressure field and thus equal in both coordinate systems. The skin friction force F_s in the total drag force F_{cd}=F_p+F_s remains also unaffected by the transformation.

To derive the expression for the modified pressure in the drop coordinate system, the pressure is integrated over the drop surface A_{ref} in the reference coordinate system, and then transformed via Φ to the surface A:

$$\begin{aligned} F_{p,ref}\left(\mathbf{u}_{ref}, p_{ref}\right) &= -\int\limits_{A_{ref}} p_{ref}\, Id\,\mathbf{n}\, dA \\ &= -\int\limits_{\Phi(A_{ref})} \left(p - \rho_c\ddot{x}_{sp}\vec{e}_x\cdot\mathbf{x}\right) Id\,\mathbf{n}\left|\det\nabla\Phi^{-1}\right| dA \end{aligned} \tag{9}$$

With $\left|\det\nabla\Phi^{-1}\right| = 1$, Eq. (9) yields:

$$\begin{aligned} F_{p,ref}\left(\mathbf{u}_{ref}, p_{ref}\right) &= -\int\limits_{\Phi(A)} p\, Id\,\mathbf{n}\, dA + \int\limits_{\text{drop}} \nabla\cdot\left(\rho_c\ddot{x}_{sp}\vec{e}_x\cdot\mathbf{x}\right) Id\, dV \\ &= F_p\left(\mathbf{u}, p\right) + M_d\frac{\rho_c}{\rho_d}\ddot{x}_{sp} \end{aligned} \tag{10}$$

The force balance in the reference system reads:

$$\mathbf{F}_{i,ref} = M_d\,\ddot{x}_{sp} = \mathbf{F}_g + \mathbf{F}_b + \mathbf{F}_s + \mathbf{F}_{p,ref} \tag{11}$$

With Eqs. (10) and (11), the acceleration force can be expressed in terms of the drop coordinate system:

$$\mathbf{F}_{i,ref} = M_d\,\ddot{x}_{sp} = \mathbf{F}_g + \mathbf{F}_b + \mathbf{F}_s + \mathbf{F}_p + M_d\frac{\rho_c}{\rho_d}\ddot{x}_{sp} = \mathbf{F}_i + M_d\frac{\rho_c}{\rho_d}\ddot{x}_{sp} \tag{12}$$

Eq. (12) is used to calculate the inlet velocity $\dot{u}_d(t) := \dot{x}_{sp}\vec{e}_x$. The inertia force $\mathbf{F}_i$ can be obtained from a standard function of STAR-CD.

This is an preprint of an article published in Chemical Engineering Science 64 (23) 4835-4845 (2009).
DOI: http://dx.doi.org/10.1016/j.ces.2009.07.023. © copyright 2009 Elsevier Ltd.

Interfacial conditions for mass transfer

In STAR-CD, each phase is calculated separately. They are related via the boundary conditons at the interface. For the simulations, the resistance of the interface to mass transfer is assumed to be negligible. The interfacial concentrations are related via the solute distribution coefficient m:

$$m = \left.\frac{c_{Ad}}{c_{Ac}}\right|_{r=R} \tag{13}$$

with continuous phase c and dispersed phase d. In general, m is a function of the solute concentration. Fig. 4 shows own experimental data for the distribution coefficient m as a function of the weight fraction of acetone in toluene. It can be seen that the distribution coefficient is constant in a preponderant part of the concentration range investigated in this study (0.001 - 3 wt-%). In the following we assume a constant value $m = 0.63$ in our numerical model.

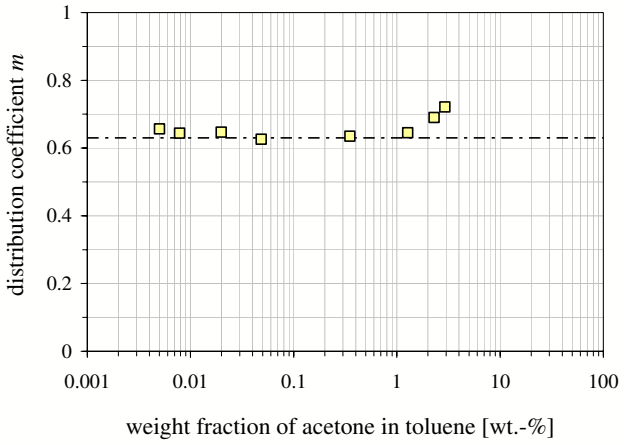

Fig. 4: Distribution coefficient m as a function of the weight fraction of acetone in toluene at 25˚C.

Across the interface, the mass fluxes are equal and according to Fick's law we can write:

$$D_{Ad} \left.\frac{\partial c_{Ad}}{\partial r}\right|_{r=R} = D_{Ac} \left.\frac{\partial c_{Ac}}{\partial r}\right|_{r=R} \tag{14}$$

In order to calculate the interfacial concentration of each cell, Eq. (14) is discretized first order using only half cell size (i.e. distance between node of the first cell adjacent to the interface and the interface itself). Due to the structure of the CFD code, the boundary condition cannot be integrated into the algorithm and thus, user subroutines have to be used. Similar to the calculation of the inlet velocity, this causes an explicit formulation and thus restrictions on the time step.

This is an preprint of an article published in Chemical Engineering Science 64 (23) 4835-4845 (2009).
DOI: http://dx.doi.org/10.1016/j.ces.2009.07.023. © copyright 2009 Elsevier Ltd.

Velocity and stress boundary conditions

The velocities at the interface are equal for both phases. Since the shape and the size of the drop are constant and the drop does not move in the coordinate system used, the radial velocities for both phases at the interface are zero:

$$u_{r,d}\big|_{r=R} = u_{r,c}\big|_{r=R} = 0 \tag{15}$$

For the tangential velocities, the continuity of velocity at the interface leads to:

$$u_{i,d}\big|_{r=R} = u_{i,c}\big|_{r=R} \qquad (i = \varphi, \Theta) \tag{16}$$

In addition to Eq. (16), the stress balance at the interface [36] is given in φ-direction by:

$$\mu_c \left(\frac{\partial u_{\varphi,c}}{\partial r} - \frac{u_{\varphi,c}}{R} \right) - \mu_d \left(\frac{\partial u_{\varphi,d}}{\partial r} - \frac{u_{\varphi,d}}{R} \right) + \frac{1}{R} \frac{\partial \sigma}{\partial \varphi} = 0 \tag{17}$$

and in Θ-direction by:

$$\mu_c \left(\frac{\partial u_{\Theta,c}}{\partial r} - \frac{u_{\Theta,c}}{R} \right) - \mu_d \left(\frac{\partial u_{\Theta,d}}{\partial r} - \frac{u_{\Theta,d}}{R} \right) + \frac{1}{R\, sin\varphi} \frac{\partial \sigma}{\partial \Theta} = 0 \tag{18}$$

The last summand on the left side of both equations includes the Marangoni stress which results from the concentration dependent interfacial tension. For convenience, the interfacial tension gradient can be written as follows:

$$\frac{\partial \sigma (c_A)}{\partial i} = \frac{\partial \sigma}{\partial c_A} \cdot \frac{\partial c_A}{\partial i} \qquad (i = \varphi, \Theta) \tag{19}$$

The expression $\partial c_A / \partial i$ can be determined based on the data available from the STAR-CD solution for the previous time step (the concentration adjacent to each boundary cell is calculated from Eq. (14)). The concentration dependence of the interfacial tension $\partial \sigma / \partial c_A$ has to be determined experimentally. In the present study, we use the experimental data published by [34]. Fig. 5 shows the absolute value of the interfacial tension gradient calculated from these experimental data. The interfacial tension gradient is approximated with a polynomial function. With this, the Marangoni stress term can be evaluated and leads to a modified interfacial tangential velocity for every affected boundary cell. Eqs. (3), (17) and (18) show the strong coupling between flow and concentration field. The governing equations are linked via these three equations. Hence, both fields have to be solved simultaneously.

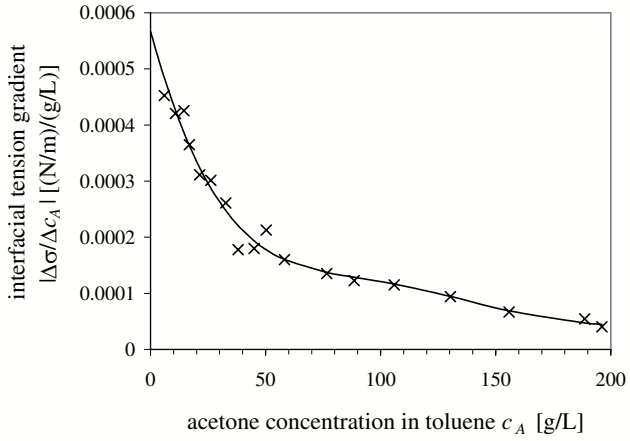

Fig. 5: Absolute value of the interfacial tension gradient $|\Delta\sigma/\Delta c_A|$ (symbols) and polynomial fit (curve). Values calculated from experimental data by Misek et al. [34].

3. Results and discussion

3.1. Terminal drop rise velocity without mass transfer

Fig. 6 shows the simulated terminal drop rise velocities as a function of drop diameter for the pure system toluene/water. For comparison, our experimental results (see Wegener et al. [33]) and data from Keith and Hixson [37] and Modigell [38] were also plotted in the figure. The agreement between our experimental data and the simulated velocities of a fluid sphere is very good for drops up to 3 *mm*. In accordance with Clift et al. [1], larger drops begin to change their shape and enter the wobbling/ellipsoidal regime and with that, the drag coefficient increases. In contrast to that, the simulations assume a perfect spherical drop shape which inevitably leads to higher values in the terminal drop rise velocity. The data by Modigell [38] are very close to the CFD simulations for a rigid drop which can only be explained with impurities in the system used in the experiments. These impurities accumulate preferably at the interface, reduce its mobility and increase the drag coefficient ([39], [40]). The data by Keith and Hixson [37] show slightly higher values for the terminal drop velocity but the velocities are still significantly lower than the data for drops with a freely moving interface.

3.2. Transient drop rise velocity with simultaneous mass transfer

In the experimental part of this study [33], the transient rise velocity for 2 *mm* toluene drops was examined with and without simultaneous mass transfer. The results indicated that Marangoni convection has strong influence on the fluid dynamic behaviour of the drop. Fig. 7 shows the typical scheme of the drop rise velocity as a function of time for later comparison with experimental results. After detachment from the nozzle tip, the drop accelerates to a first plateau if Marangoni convection is strong enough. In this case, Marangoni induced tangential shear forces occur leading to interfacial convections which can also be opposite to the external flow. Thus,

This is an preprint of an article published in Chemical Engineering Science 64 (23) 4835-4845 (2009).
DOI: http://dx.doi.org/10.1016/j.ces.2009.07.023. © copyright 2009 Elsevier Ltd.

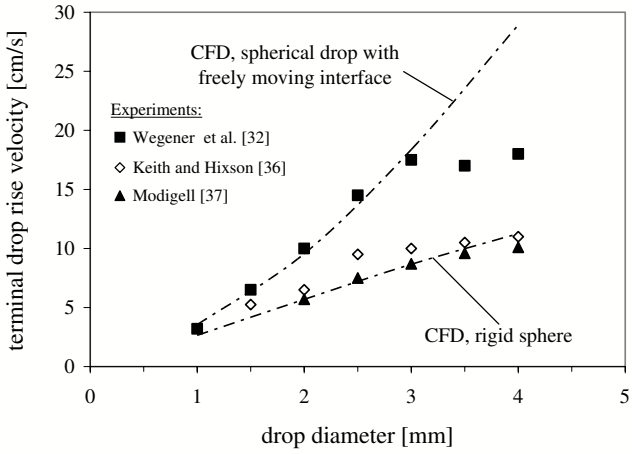

Fig. 6: Terminal rise velocity of toluene drops in water as a function of the drop diameter. Comparison of experimental results ([33], [38], [37]) with simulation results of a rigid sphere and a drop with freely moving interface.

the relative velocity decreases and the drag force increases. The higher the initial concentration is, the stronger are Marangoni phenomena and the lower is the plateau velocity. For initial concentrations higher than a certain value, the plateau velocity is equal to the terminal velocity of a correspondent rigid sphere. Higher initial concentrations do not lead to lower plateau velocities than the terminal velocity for the rigid sphere. After a certain mass transfer time t_{rac}, the influence of Marangoni convection gets weaker due to the lower concentration level. Consequently, the possible concentration gradients are smaller which are the main driving force for Marangoni convection. The interfacial movements opposite to the external flow decay and the inner circulation can develop. Thus, the drop reaccelerates to the terminal velocity u_t. The higher the initial concentration is, the higher is t_{rac}. If the initial concentration is low enough, u_t is reached without any intermediate plateau. Our experimental investigations showed that u_t is slightly lower compared to the terminal velocity of an initially unloaded drop ($u_{t,\sigma=const.}$) which is probably due to the fact that the mass transfer is not fully completed and Marangoni convection still takes place, but on a very low level. More detailed results concerning the two-step acceleration behaviour in case of Marangoni convection can be found in Wegener et al. [41].

In Fig. 8, the simulated drop rise velocity for different initial solute concentrations is shown. For comparison, the limiting curve for the rigid sphere is given in the figure. The results show good qualitative agreement with the development of values described in Fig. 7. For $c_{A,0} = 15$ and $30\,g/L$ the drop accelerates to the terminal velocity of a rigid sphere first. The reacceleration begins the later the higher the initial concentration is. For lower initial concentrations, the influence of Marangoni convection is weaker but still strong enough to stabilize the drop at a lower intermediate velocity level compared to the unloaded drop ($\sigma = const.$). For concentrations lower than $1.8\,g/L$, the rise velocity shows practically no delay, the drop accelerates immediately to a constant value.

This is an preprint of an article published in Chemical Engineering Science 64 (23) 4835-4845 (2009).
DOI: http://dx.doi.org/10.1016/j.ces.2009.07.023. © copyright 2009 Elsevier Ltd.

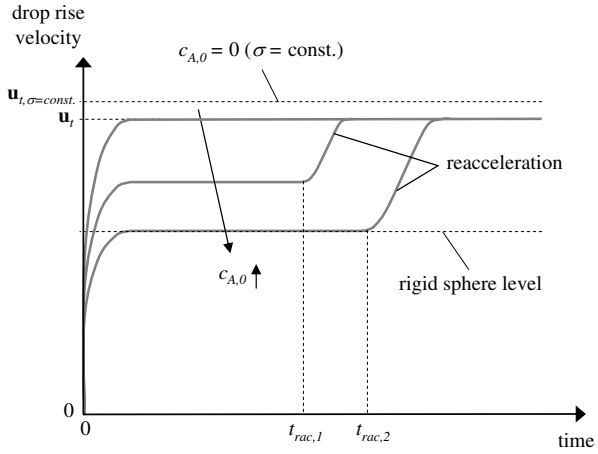

Fig. 7: Schematic of the two-step acceleration behaviour in case of Marangoni convection. The relative velocity is plotted as a function of time for different initial solute concentrations $c_{A,0}$. For higher $c_{A,0}$, the drop accelerates in a first step to the velocity level of a rigid sphere, for moderate concentrations to an intermediate plateau and for lower concentrations directly to a constant velocity level. This velocity is significantly lower than in the case of constant interfacial tension.

The velocity after reacceleration for all cases with Marangoni convection – independently from the temporal development of each curve – is lower than for the case with constant interfacial tension, a fact which has been shown in the experiments as well [33]. According to the discussion of Fig. 7, the simulations reveal that there has to be Marangoni influence left since the concentration is low but significantly higher than zero. This can be explained with Fig. 5: even for very small concentrations the interfacial tension gradient has a certain value. The difference in the velocities (around 100 mm/s instead of 105 mm/s) is significant since the numerical error is smaller than 5%.

For higher initial solute concentrations, the curves show oscillations which can be attributed to two main effects: local Marangoni structures and model restrictions. Local Marangoni structures have a real physical meaning, and thus interfacial instabilities are able to change the sign of the local interfacial velocity. More contributions opposite to the external flow increase the drag and retard the drop, whereas less contributions lead to a drop acceleration. This can change abruptly due to the inherently chaotic structure of the Marangoni convections and would consequently lead to oscillations. In terms of model restrictions, a straight vertical pathway is imposed, i.e. horizontal movements in the y, z-plane caused by pressure gradients are not possible. Therefore, inaccuracies in the computed relative velocity must be assumed.

Fig. 9 compares experimental [33] and simulated drop rise velocities for selected initial concentrations. The case without solute is given for comparison. In this case, the quantitative agreement in the acceleration behaviour is very good and the terminal velocity value is exactly reproduced. If acetone is added, the qualitative behaviour of numerical and experimental results agrees well. In terms of the reacceleration time however, simulation results differ from the exper-

This is an preprint of an article published in Chemical Engineering Science 64 (23) 4835-4845 (2009).
DOI: http://dx.doi.org/10.1016/j.ces.2009.07.023. © copyright 2009 Elsevier Ltd.

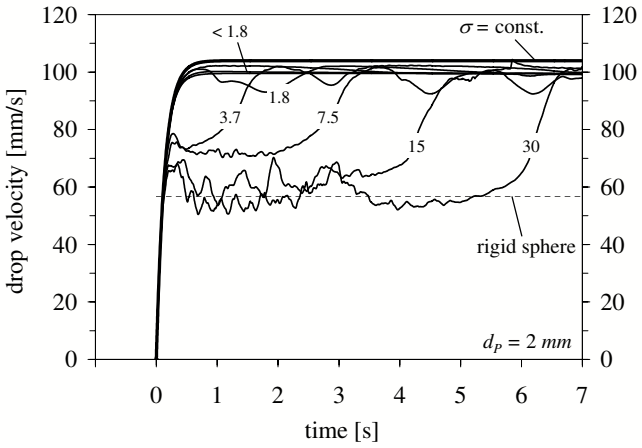

Fig. 8: Simulated drop rise velocity as a function of time for different initial solute concentrations (in g/L). The velocity of a rigid sphere is given for comparison.

iments. In the experiments, the reacceleration begins significantly later than in the simulations, i.e. the influence of Marangoni convection is predominant for a longer period of time in the experiment than in the simulation. This could probably be due to both experimental and modelling effects. From the numerical point of view, some of the experimental phenomena were not considered in the simulations, such as drop deformation, oscillation, changes in particle path, and changes in density and viscosity ratio. Deformation or oscillation effects tend to promote mass transfer, thus Marangoni convection would decay earlier, and the reacceleration time would shift to even smaller times. On the other hand, it is known from the experiments that drop deformation/oscillation is small for 2 *mm* droplets. Changes in particle path occur with the reacceleration in the experiments, before, the droplets rise vertically, and thus the model simplification 6 in chapter 2.1 holds. Lastly, density and viscosity effects are small due to the relatively low concentration level. Thus, the reason of the deviations in reacceleration time between simulations and experiments remain unclear and further investigations are needed to investigate the different impacts on this issue.

3.3. Mass transfer

In this section, the numerical results concerning the influence of the initial concentration on mass transfer are presented and finally compared with experimental results by Wegener et al. [33]. Fig. 10 shows the simulated dimensionless mean concentration $c^* = \overline{c}_A/c_{A,0}$ as a function of time. All simulation results lie between two limiting curves: for $\sigma = const.$, we have the conjugated problem without Marangoni convection. In this case, the development of c^* with time is equal for all initial concentrations $c_{A,0}$ since an increase in $c_{A,0}$ will increase $\overline{c}_A$ likewise. The mass transfer is lower than in all other cases $\sigma \neq const$. The second curve represents the "external problem". In this case, there is no mass transfer resistance inside the drop (perfect mixing, $D_{Ad} \rightarrow \infty$). Mass transfer is therefore higher compared to the other cases.

This is an preprint of an article published in Chemical Engineering Science 64 (23) 4835-4845 (2009).
DOI: http://dx.doi.org/10.1016/j.ces.2009.07.023. © copyright 2009 Elsevier Ltd.

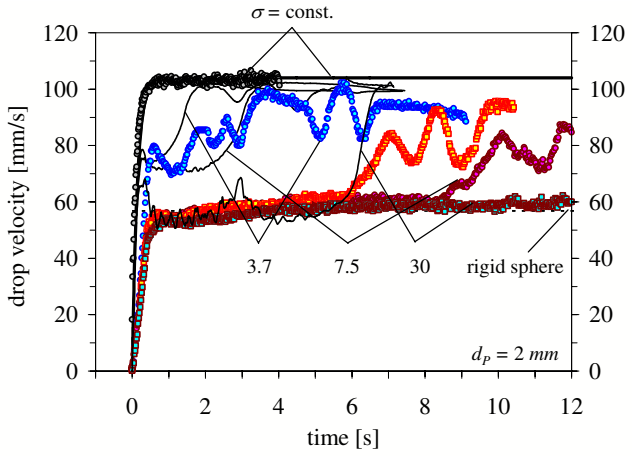

Fig. 9: Comparison between selected experimental (symbols) [33] and simulated (curves) drop rise velocities as a function of time for different initial solute concentrations (in g/L).

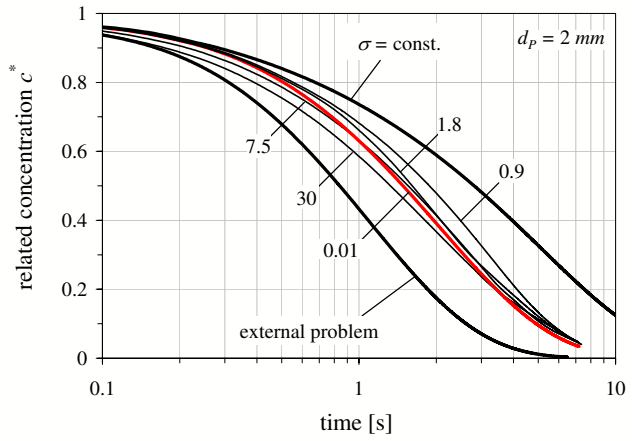

Fig. 10: Simulated dimensionless mean solute concentration c^* as a function of time for different initial solute concentrations (in g/L).

If the initial solute concentration is increased from $0.9\,g/L$ to $30\,g/L$, the c^*-curves shift to the left. Marangoni convection gets stronger, the internal mixing is promoted and mass transfer is increased. Of course, mass transfer outside the droplet is affected as well, but external resistance against mass transfer is already small compared to the internal resistance due to the high Peclet number ($> 5 \cdot 10^4$) and thus relatively thin boundary layer.

The situation is different for lower concentrations: if $c_{A,0}$ is below $0.9\,g/L$, the curves are not shifted further to the right, but to the left again (the $0.1\,g/L$-curve only differs slightly from

This is an preprint of an article published in Chemical Engineering Science 64 (23) 4835-4845 (2009).
DOI: http://dx.doi.org/10.1016/j.ces.2009.07.023. © copyright 2009 Elsevier Ltd.

the $0.01\,g/L$-curve and is not plotted in the figure). This indicates that the mass transfer rate has a minimum at $0.9\,g/L$. This interesting result was qualitatively confirmed in the experiments by Wegener et al. [33] (the minimum there was at $c_{A,0} \approx 5\,g/L$) and reveals the sophisticated interaction of concentration and velocity field due to Marangoni convection.

Fig. 11 highlights this issue in more detail. The time where 50% of the mass transfer is completed, t_{50}, is plotted versus $c_{A,0}$. Analogous to the experimental results, the figure can be divided in two sections. In the first section ($c_{A,0} < 0.9\,g/L$), the drop almost immediately accelerates to its terminal drop rise velocity as shown in Fig. 8. This implies that the internal circulation can develop and thus the Reynolds number is larger for a longer period of time compared to higher initial concentrations. In terms of mass transfer however, significant effects must occur since c^* decreases much faster than for $\sigma = const$. This result suggests that mass transfer is dominated by both the internal circulation and Marangoni convection structures.

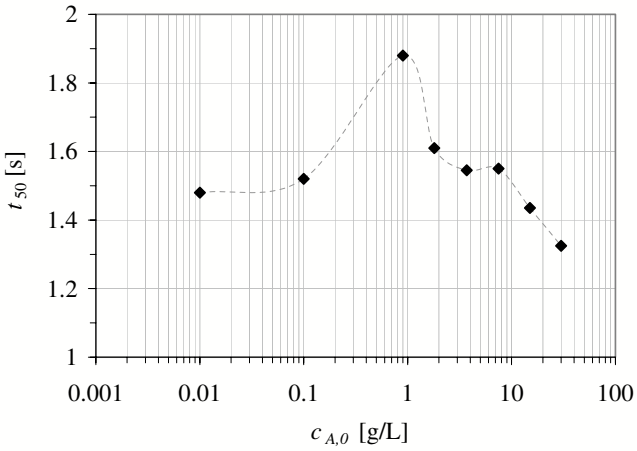

Fig. 11: Simulated time t_{50} as a function of the initial solute concentration $c_{A,0}$.

In the transition region between $c_{A,0} = 0.1$ and $1.8\,g/L$, Marangoni convection slowly gets stronger, increases the drag coefficient and therewith decreases the drop rise velocity or the Reynolds number respectively. Obviously, the stronger Marangoni convection cannot overcompensate the reduction of the Reynolds number, leading to slightly higher t_{50}.

In the right hand section, the Marangoni effect becomes more and more dominant. Despite the temporarily lower drop rise velocity (and therewith lower Reynolds numbers), the Marangoni structures are effective and strong enough to overcompensate the "interfacial blockage effect" [33] which describes in few words the replacement of the internal toroidal flow pattern by chaotic Marangoni structures and the associated increase of the drag coefficient. Obviously, the higher the concentration is, the better is radial mixing and the lower is the internal mass transfer resistance. Therefore, the values tend towards the external problem which seems to be a limit at least for the investigated system. In contrast to the experiments, where the system with constant interfacial tension does not exist, the enhancement factor $E = t_{50,\sigma=const.}/t_{50}$ with $t_{50,\sigma=const.} = 2.84$ can

This is an preprint of an article published in Chemical Engineering Science 64 (23) 4835-4845 (2009).
DOI: http://dx.doi.org/10.1016/j.ces.2009.07.023. © copyright 2009 Elsevier Ltd.

be calculated from the simulations and ranges between 1.7 and 2.5 for all concentrations. This is in good agreement with experiments showing enhancement factors > 2 for all concentrations investigated. Thus, mass transfer is, compared to $\sigma = const.$, always enhanced if Marangoni convection occurs, independently of the initial concentration. Even for very low concentrations, Marangoni instabilities contribute significantly to the shear stress balance in the Eqs. 17 and 18, and thus play a significant role in the process.

This main result can be discussed based on Fig. 12 which shows the simulated concentration fields for three different cases ($\sigma = const.$, $c_{A,0} = 0.9\,g/L$ and $c_{A,0} = 30\,g/L$) at two different dimensionless mean concentrations c^* (0.9 and 0.3). The inlet-flow points to the negative x-direction (or the drop rises in the positive x-direction) according to Fig. 2. On the left hand side of each plot, the x,z-plane shows the axial concentration field, whereas in the y,z-plane the radial patterns perpendicular to the inlet-flow are displayed.

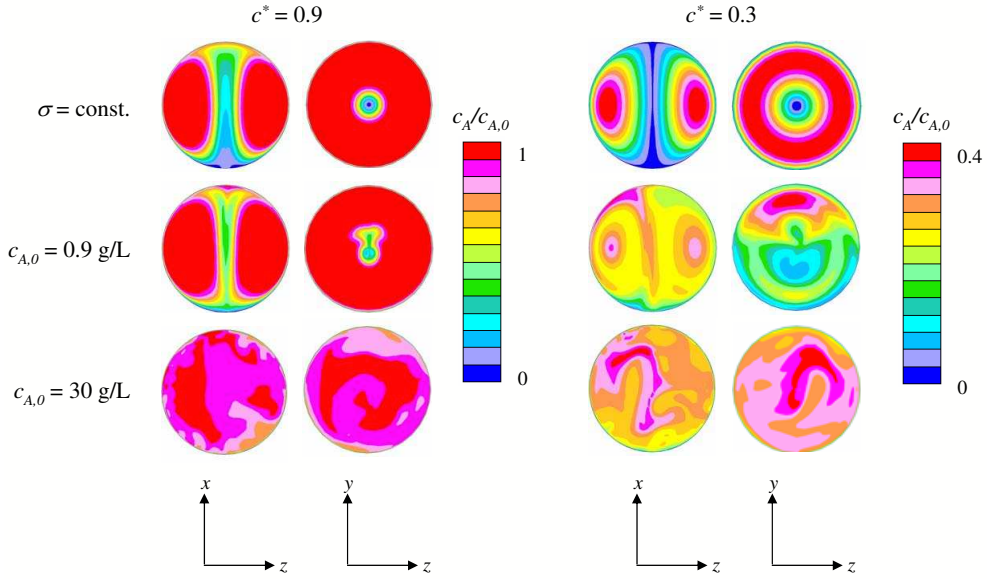

Fig. 12: Simulated concentration plots (drop only) for three different initial concentrations at $c^* = 0.9$ (left) and at $c^* = 0.3$ (right) in two different views. x,z-plane: view parallel to the flow, y,z-plane: view perpendicular to the flow. The coordinate system is analogue to Fig. 2.

When no Marangoni convection occurs ($\sigma = const.$), the typical toroidal axis-symmetric flow pattern is developed. The radial view shows the corresponding concentric concentration rings. The transport of matter perpendicular to the concentration isolines is only due to molecular diffusion. For low initial concentrations ($c_{A,0} = 0.9\,g/L$, $\sigma \neq const.$), some significant differences can be stated. The axial flow is not symmetric, e.g. for $c^* = 0.3$, the concentration gradients are smaller, and thus the concentration field is more even compared to $\sigma = const.$ Regarding the radial direction, it can be seen that the concentric rings disappear and more or less chaotic convective patterns develop which lead to higher radial mixing. Also in this direction,

This is an preprint of an article published in Chemical Engineering Science 64 (23) 4835-4845 (2009).
DOI: http://dx.doi.org/10.1016/j.ces.2009.07.023. © copyright 2009 Elsevier Ltd.

the concentration gradients are smaller. These results suggest that even for very low initial concentrations, Marangoni convection generates complex convective flow patterns which enhance mass transfer significantly.

When the initial concentration is increased (here $c_{A,0} = 30\,g/L$), the toroidal structure disappears right from the start. The Marangoni effect leads to highly eruption-like patterns which extend quickly into the drop. Interestingly, the axial and radial concentration patterns are very similar to one another which emphasizes the chaotic and fully 3D character in the whole flow. Fig. 13 shows the corresponding concentration field for $c_{A,0} = 30\,g/L$ in the surrounding fluid in the x,z-plane for two different c^*. The effect of the Marangoni structures can clearly be identified. Generally, the structures are more pronounced at the rear of the drop. In the earlier stage of the process, when $c^* = 0.9$ and the Reynolds number is still small, the Marangoni structures develop on a sub-drop scale similar to roll cell patterns along the surface. Instabilities do occur at the front stagnation point as well, but they are quickly transported downstream.

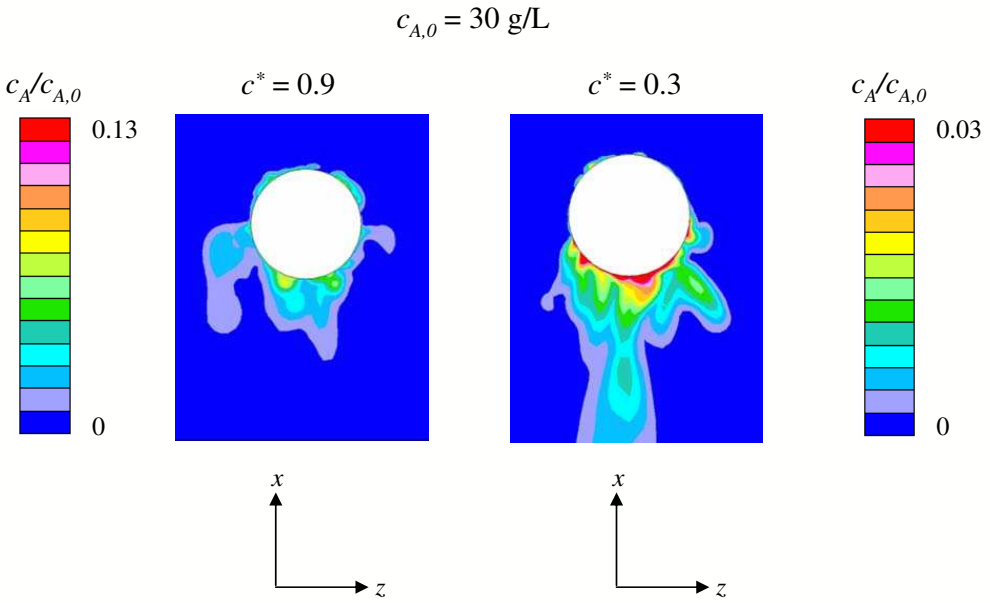

Fig. 13: Simulated concentration plots (surrounding only) for $c_{A,0} = 30\,g/L$ at $c^* = 0.9$ (left) and at $c^* = 0.3$ (right) in the x,z-plane (view parallel to the flow). The coordinate system is analogue to Fig. 2.

Lastly, Fig. 14 compares simulation results with experimental data by Wegener et al. [33]. For convenience, only two initial concentrations were selected ($c_{A,0} = 1.8$ and $30\,g/L$). The figure shows reasonable quantitative agreement between simulations and experiments despite the differences in the description of the drop rise velocity.

Finally, let us critically review the model simplifications from Section 2.1 and their poten-

This is an preprint of an article published in Chemical Engineering Science 64 (23) 4835-4845 (2009).
DOI: http://dx.doi.org/10.1016/j.ces.2009.07.023. © copyright 2009 Elsevier Ltd.

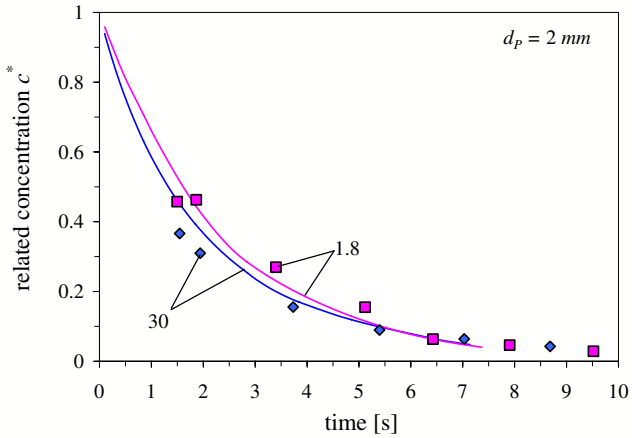

Fig. 14: Simulated dimensionless mean solute concentration c^* as a function of time (lines) compared with experimental results (symbols) [33].

tial implications on the results and the above mentioned discrepancies. Assumptions 2. and 3. are without doubt feasible for the system under consideration, likewise Assumption 4. for a clean laboratory environment. Since non-isothermal effects do not play a crucial role and the concentrations are low, also Assumption 5. is realistic.

Clearly, Assumption 1. is only valid as long as the drop diameter is small (or Weber number below the critical value 4). For larger drops, there are definitely deformations of the drop and also even onset of wobbling. These effects do have a strong influence on the dynamics of the rise of the drop. However, our current numerical method is not capable of coping with these deformations.

Likewise (but less important in our view), Assumption 6. (assuming a vertical path) is violated for larger drops and higher concentrations. It is clear, how deformations change the drop dynamics qualitatively. The mechanism and effects of a three dimensional path way are less clear to us. However, changes of the path way only start after strong deformations have occurred and might be thus considered as a secondary effect.

This is an preprint of an article published in Chemical Engineering Science 64 (23) 4835-4845 (2009).
DOI: http://dx.doi.org/10.1016/j.ces.2009.07.023. © copyright 2009 Elsevier Ltd.

4. Conclusions

An intense 3D numerical study of the fluid dynamic behaviour and the mass transfer characteristics in the toluene/aceton/water system with simultaneous Marangoni convection has been carried out. Velocity and concentration fields were solved simultaneously in a moving reference coordinate system. The additional Marangoni stress has been implemented via the discretized stress boundary conditions extended by the interfacial tension gradient. For comparison and validation of the numerical results, own experimental data [33] are available.

Simulations of the terminal drop rise velocity without accompanied mass transfer show excellent agreement with experimental results as long as

- the used fluids and materials are of high purity in the experiments,
- the drops are sufficiently spherical (i.e. small shape oscillations).

In the case of Marangoni convection, the simulations show quantitatively good agreement with experimental results concerning fluid dynamics in the following points:

- For low initial solute concentrations, the terminal velocity is reached without intermediate step, but it is lower than the terminal velocity of an unloaded drop.
- If Marangoni convection is strong enough, an intermediate velocity level is reached which is the lower the higher the initial concentration is.
- The lowest intermediate velocity level is that of a rigid sphere.
- The onset of reacceleration is the later the higher the initial concentration is.

Nevertheless, there are some quantitative discrepancies if the numerical results are compared with the experimental results:

- The reacceleration in the experiments for the same initial concentration starts later than in the simulations.
- In the experiments, the influence of Marangoni convection on the drop rise velocity begins with lower initial concentrations than in the simulations.

Concerning mass transfer, the dimensionless concentration c^* has been used in order to verify the accordance between simulations and experiments. Again, reasonable good agreement can be stated. The simulated mass transfer rate is the nearer to the external problem the higher the initial concentration is and it is never lower than in the case where the interfacial tension is constant. Obviously, there is a complex interaction between internal circulation and Marangoni convection structures, and thus their influence on the mass transfer rate is complex as well. It can be summarized that

- mass transfer is always enhanced compared to the case $\sigma = const.$, independently from the initial solute concentration,
- mass transfer enhancement is around factor 2,
- in a certain concentration range the internal circulation is hindered due to the ”blockage effect” of incipient Marangoni structures. In this concentration range, the mass transfer rate decreases when initial solute concentration is increased,

- there is good quantitative agreement between simulations and experiments in the development of c^*.

The objective of future work will be to obtain generalized correlations in order to describe the mass transfer with accompanied Marangoni convection reliably. Thereto, more experimental and numerical investigations are needed in order to improve our physical understanding of the complex phenomena. Intense parameter studies varying drop diameter, mass transfer direction, viscosity ratio and others are currently under way.

Moreover, there is need for further development of numerical methods in order to incorporate first of all drop deformations and then also to abandon the assumption of a vertical drop motion.

Acknowledgement

The authors like to acknowledge the German Research Foundation (DFG) for financial support. The simulations were performed on the IBM pSeries 690 Supercomputer provided by "The North-German Supercomputing Alliance (HLRN)". We would like to thank the staff members for their support. Furthermore, the comments of one of the reviewers are gratefully acknowledged. They led to a significant improvement of the manuscript.

5. Notation

Latin letters

a	acceleration, m/s^2
A	drop surface, m^2
c	concentration, kg/m^3
$\overline{c}$	mean concentration, kg/m^3
c^*	dimensionless mean concentration, dimensionless
d_P	drop diameter, m
D	molecular diffusivity, m^2/s
$\vec{e}_x$	unit vector, dimensionless
E	enhancement factor, dimensionless
F	force, $kg\,m/s^2$
g	gravitational acceleration, m/s^2
h	height, m
Id	identity matrix
m	distribution coefficient, dimensionless
M	mass of the drop, kg
$\mathbf{n}$	normal vector
p	pressure, $kg/(ms^2)$
r	radial coordinate, m
R	drop radius, m
t	time, s
$\mathbf{u}$	velocity, m/s
u_i	velocity component, m/s
V	drop volume, m^3
x, y, z	Cartesian coordinates, m

Greek letters

Θ azimuth angle
ϑ temperature, $^{\circ}C$
μ dynamic viscosity, $Pa\,s$
ρ density, kg/m^3
σ interfacial tension, N/m
φ zenith angle

Subscripts

A solute
$A,0$ initial solute
b buoyancy
c continuous phase
cd drag coefficient
col column
cr critical
cyl cylinder
d dispersed phase, drop
g gravitation
i inertia
p pressure
r radial
rac reacceleration
ref reference coordinate system
s skin friction
t terminal

Miscellaneous

Φ coordinate transformation from reference to drop coordinate system

References

[1] Clift, R.; Grace, J.R.; Weber, M.E.: *Bubbles, Drops, and Particles*, Academic Press, New York (1978)
[2] Handlos, A.E.; Baron, T.: *Mass and Heat Transfer from Drops in Liquid-Liquid Extraction*, AIChE Journal, **3(1)**, 127-136 (1957)
[3] Kronig, R.; Brink, J.C.: *On the Theory of Extraction from Falling Droplets*, Applied Scientific Research Section a-Mechanics Heat Chemical Engineering Mathematical Methods, **2(2)**, 142-154 (1950)
[4] Newman, A.B.: *The drying of porous solid. Diffusion and surface emission effects*, Trans. AIChE **27(203-216)** (1931)
[5] Ruckenstein, E.: *Mass transfer between a single drop and a continuous phase*, International Journal of Heat and Mass Transfer, **10(12)**, 1785-1792 (1967)
[6] Brauer, H.: *Unsteady state mass transfer through the interface of spherical particles–II : Discussion of results obtained by theoretical methods*, International Journal of Heat and Mass Transfer, **21(4)**, 455-465 (1978)
[7] Plöcker, U.J.; Schmidt-Traub, H.: *Instationärer Stoffbergang zwischen einer Einzelkugel und einer ruhenden Umgebung*, Chemie Ingenieur Technik, **44(5)**, 313-319 (1972)
[8] Piarah, W.H.; Paschedag, A.; Kraume, M.: *Numerical simulation of mass transfer between a single drop and an ambient flow*, AIChE Journal, **47(7)**, 1701-1704 (2001)
[9] Paschedag, A.R.; Piarah, W.H.; Kraume, M.: *Sensitivity study for the mass transfer at a single droplet*, International Journal of Heat and Mass Transfer, **48(16)**, 3402-3410 (2005)
[10] Waheed, A.; Henschke, M.; Pfennig, A.: *Mass transfer by free and forced convection from single spherical liquid drops*, International Journal of Heat and Mass Transfer, **45(22)**, 4507-4514 (2002)
[11] Favelukis, M.; Ly, C.H.: *Unsteady mass transfer around spheroidal drops in potential flow*, Chemical Engineering Science, **60(24)**, 7011-7021 (2005)
[12] Petera, J.; Weatherley, L.R.: *Modelling of mass transfer from falling droplets*, Chemical Engineering Science, **56(16)**, 4929-4947 (2001)
[13] Bothe, D.; Koebe, M.; Warnecke, H.-J.: *VOF-Simulation of the rise behaviour of single air bubbles with oxygen transfer to the ambient liquid*, Transport Phenomena with moving Boundaries, Berlin, (2004)
[14] Koebe, M.: *Numerische Simulation aufsteigender Blasen mit und ohne Stoffaustausch mittels der Volume of Fluid (VOF) Methode*, PhD thesis (2004)
[15] Dijkhuizen, W.; van Sint Annaland, M.; Kuipers, H.: *Numerical investigation of closures for interface forces in dispersed flows using a 3D front tracking model*, 4th International Conference on CFD in the Oil and Gas, Metallurgical & Process Industries. SINTEF / NTNU, Trondheim, Norway (2005)
[16] Tryggvason, G.; Bunner, B.; Esmaeeli, A.; Juric, D.; Al-Rawahi, N.; Tauber, W.; Han, J.; Nas, S.; Jan, Y.J.: *A Front-Tracking Method for the Computations of Multiphase Flow*, Journal of Computational Physics, **169(2)**, 708-759 (2001)
[17] Darmana, D.; Deen, N. G.; Kuipers, J.A.M.: *Detailed 3D Modeling of Mass Transfer Processes in Two-Phase Flows with Dynamic Interfaces*, Chemical Engineering & Technology, **29(9)**, 1027-1033 (2006)
[18] Darmana, D.; Dijkhuizen, W.; Deen, N.G.; van Sint Annaland, M.; Kuipers, J.A.M.: *Detailed 3D Modelling of Mass Transfer Processes in Two Phase Flows with Dynamic Interfaces*, International Conference on Multiphase Flow, Ed. Sommerfeld, M., Leipzig, Germany (2007)
[19] Koynov, A.; Khinast, J.G.; Tryggvason, G.: *Mass Transfer and Chemical Reactions in Bubble Swarms with Dynamic Interfaces*, AIChE Journal, **51(10)**, 2786-2800 (2005)
[20] Mao, Z.-S.; Li, T.; Chen, J.: *Numerical simulation of steady and transient mass transfer to a single drop dominated by external resistance*, International Journal of Heat and Mass Transfer, **44(6)**, 1235-1247 (2001)
[21] Yang, C.; Mao, Z.-S.: *Numerical simulation of interphase mass transfer with the level set approach*, Chemical Engineering Science, **60(10)**, 2643-2660 (2005)
[22] Wang, J.; Lu, P.; Wang, Z.; Yang, C.; Mao, Z.-S.: *Numerical simulation of unsteady mass transfer by the level set method*, Chemical Engineering Science, **63(12)**, 3141-3151 (2008)
[23] Kruijt-Stegeman, Y.W.; van de Vosse, F.N.; Meijer, H.E.H.: *Droplet behaviour in the presence of insoluble surfactants*, Physics of Fluids, **16(8)**, 2785-2796 (2004)
[24] Cuenot, B.; Magnaudet, J.; Spennato, B.: *The Effects of slightly soluble surfactants on the flow around a spherical bubble*, J. Fluid Mech., **339(25-53)** (1997)
[25] Li, X.; Mao, Z.-S.; Fei, W.: *Effects of surface-active agents on mass transfer of a solute into single buoyancy driven drops in solvent extraction systems*, Chemical Engineering Science, **58(16)**, 3793-3806 (2003)
[26] Sawistowski, H.: in:*Recent Advances in Liquid-Liquid Extraction*, Ed. C. Hanson, Pergamon Press, 293-365 (1971)
[27] James, A.J.; Lowengrub, J.: *A surfactant-conserving volume-of-fluid method for interfacial flows with insoluble surfactant*, J. of Comp. Phys, **201(685-722)** (2004)
[28] Wang, Y.P.; Papageorgiou, D.T.; Maldarelli, C.: *Increased mobility of a surfactant-retarded bubble at high bulk concentrations*, Journal of Fluid Mechanics, **390(251-270)** (1999)

[29] Mao, Z.-S.; Chen, J.: *Numerical simulation of the Marangoni effect on mass transfer to single slowly moving drops in the liquid-liquid system*, Chemical Engineering Science, **59(8-9)**, 1815-1828 (2004)
[30] Sternling, C.V.; Scriven, L.E.: *Interfacial turbulence: hydrodynamic instability and the Marangoni effect*, AIChE Journal, **5(4)**, 514-523 (1959)
[31] Huo, Y.; Li, B.Q.: *Three-dimensional Marangoni convection in electrostatically positioned droplets under microgravity*, International Journal of Heat and Mass Transfer, **47(14-16)**, 3533-3547 (2004)
[32] Wegener, M.; Paschedag, A.R.; Kraume, M.: *Experimentelle Untersuchungen sowie 2D- und 3D-Simulationen zum Stofftransport an Einzeltropfen mit Marangoni-Konvektion*, Chemie Ingenieur Technik, **79(1-2)**, 73-81 (2007)
[33] Wegener, M.; Grünig, J.; Stüber, J.; Paschedag, A.R.; Kraume, M.: *Transient rise velocity and mass transfer of a single drop with interfacial instabilities - experimental investigations*, Chemical Engineering Science, **62(11)**, 2967-2978 (2007)
[34] Misek, T.; Berger, R.; Schröter, J.: *Standard test systems for liquid extraction*, Inst. Chem. Eng., EFCE Publication Series, 46 (1985)
[35] CD-adapco group: *Methodology STAR-CD v3.20* (2004)
[36] Deen, W.M.: *Analysis of transport phenomena*, Oxford University Press, Oxford, New York (1998)
[37] Keith, F.W.; Hixson, A.N.: *Liquid-Liquid Extraction Spray Columns-Drop formation and interfacial transfer area*, Industrial and Engineering Chemistry, **47(2)**, 258-267 (1955)
[38] Modigell, M.: *Untersuchung der Stoffübertragung zwischen zwei Flüssigkeiten unter Berücksichtigung von Grenzflächenphänomenen*, PhD thesis RWTH Aachen (1981)
[39] Edge, R.M.; Grant, C.D.: *The terminal velocity and frequency of oscillation of drops in pure systems*, Chemical Engineering Science, **26(7)**, 1001-1012 (1971)
[40] Edge, R.M.; Grant, C.D.: *The motion of drops in water contaminated with a surface-active agent*, Chemical Engineering Science, **27(9)**, 1709-1721 (1972)
[41] Wegener, M.; Fevre, M.; Paschedag, A.R.; Kraume, M.: *Impact of Marangoni instabilities on the fluid dynamic behaviour of organic droplets*, International Journal of Heat and Mass Transfer, **52(11-12)**, 2543-2551 (2009)